Two-Dimensional High-Efficiency Transceiver Integrated Optical Phased Array With Dual-Port Antenna

Yaoyuan Zhang, Rui Wang, and Ming Wei

***Abstract*—We propose a 1 × 32 silicon photonics transceiver integrated optical phased array (OPA) with a large scanning angle. It can process receive and transmit signals simultaneously, which effectively increases the on-chip signal transmission efficiency. The simulation shows that the phase-tuned 62.2° lateral beam steering without grating lobe and the wavelength-tuned 31.2° longitudinal beam steering can be achieved in the transmitting mode, and the overall optical loss is less than 9.1 dB. In the receiving mode, the combination of the two detection methods reduces the complexity of the system while ensuring the sensitivity of the system. According to statistics, an effective collection area of 43.3% per unit area can be achieved in the receiving mode, which provides a reliable guarantee for subsequent high-quality signal processing.**

***Index Terms*—Optical phased array, transceiver integration, silicon photonics integration, beam steering.**

I. Introduction

IT IS extremely important to achieve accurate control of the beam steering for most of the current optical systems. Most of the traditional structures use lenses or mechanical structures to achieve beam control, but the traditional solutions are relatively cumbersome and costly. Therefore, the silicon-based optical phased array (OPA) offers a solution to this problem. Integrated OPA has been extensively studied due to its solid-state beam steering capability [1], [2], which has promising applications in laser detection and ranging (LiDAR) [3], free-space optical communications [4], and laser displays [5]. OPAs can accurately steer the beam by precisely controlling the phase of each array element. In recent years, a large number of studies have been carried out on the emission structure of OPAs. There are two ways to achieve two-dimensional scanning of OPA, one-dimensional linear array structure combined with wavelength tuning [6], [7], [8] and two-dimensional precision control [9] for each antenna element by designing a two-dimensional antenna array. On this basis, non-uniform arrays optimized by various algorithms are proposed to enhance the directivity of OPAs [10], [11]. At the same time, the receiving OPA module can collect light from any desired direction selectively. It can also reject unwanted light from other directions, multipath reflections, and even active jammers. These spatially selective receptions are of great value in many applications. In the previous literature [12], they reported the first monolithic OPA transceiver with independent control of amplitude and phase for each element. However, this structure directly detects the optical signal based on the reciprocity of the optical path and is easily affected by other interference sources due to the weak received signal. At the same time, there have been reports on the coherent reception of OPAs in recent years [13]. Coherent detection can improve the detection sensitivity, and it can realize the directional detection of the optical signal at the same time. Studies have shown that the antenna elements need to maintain a certain distance to avoid excessive crosstalk, so a large amount of energy will inevitably enter the substrate in the receiving process. As a result, within the controllable range of crosstalk between antennas, the denser the antenna array is, the stronger the optical power received by the antenna. At present, the antenna size of the two-dimensional antenna array is relatively small, and the two-dimensional antenna array is usually designed with the phase shifter close to the antenna, which will inevitably lead to a small fill factor of the antenna array. The one-dimensional antenna array structure has a relatively large antenna size, and the phase-modulator does not need to be in close contact with the antenna structure, so the array fill factor is larger than the 2D arrays.

In this paper, we propose a large-angle two-dimensional transceiver integrated OPA. It can double the antenna field of view by antenna counter-incidence combined with wavelength tuning. The structure can process receive and transmit signals simultaneously, which effectively increases the on-chip signal transmission efficiency. While it can realize the independent switching of OPA reception and transmission functions by controlling the on-off of the optical path through the Mach-Zehnder optical switch which improves the degree of freedom of on-chip control and the efficiency of signal transmission. At the same time, it can improve the on-chip integration effectively compared to traditional transceiver discrete structures. The simulation

Manuscript received 12 July 2022; revised 6 August 2022; accepted 9 August 2022. Date of publication 16 August 2022; date of current version 29 August 2022. This work was supported by the Capital Construction Fund within the budget of Jilin Province in 2022 under Grant 2022C046-2. *(Corresponding author: Rui Wang.)*

Yaoyuan Zhang and Ming Wei are with the Changchun Institute of Optics, Fine Mechanics and Physics, Chinese Academy of Sciences, Changchun 130033, China, and also with the University of Chinese Academy of Sciences, Beijing 100049, China (e-mail: zhangyaoyuan19@mails.ucas.ac.cn; weiming19@mails.ucas.ac.cn).

Rui Wang is with the Changchun Institute of Optics, Fine Mechanics and Physics, Chinese Academy of Sciences, Changchun 130033, China (e-mail: darui9999@163.com).

Digital Object Identifier 10.1109/JPHOT.2022.3199043

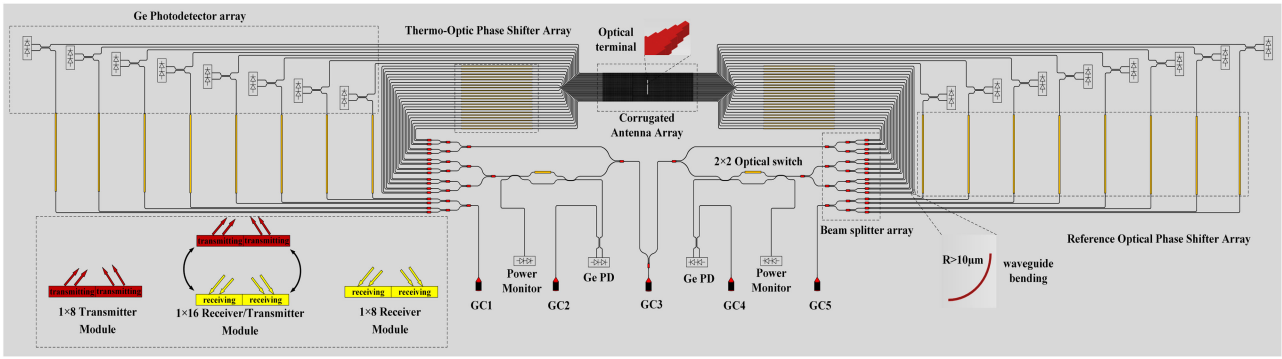

Fig. 1. Schematic diagram of the integrated structure of the OPA transceiver.

results show that the longitudinal steering angle of 31.2° can be achieved by wavelength tuning of the dual-port antenna in transmit mode, and the lateral steering angle of 62.2° can be achieved by phase adjustment. What's more, the overall optical loss is lower than 9.1 dB. In the receiving mode, we combine the two receiving methods, which can improve the accuracy of the received signal as much as possible while ensuring the receiving sensitivity. For the receiving antenna, we utilize the one-dimensional corrugated antenna to maximize the antenna receiving efficiency while ensuring the scanning angle. Statistics show that it can achieve an effective collection area of 43.3% of the unit receiving area, which provides a reliable guarantee for the high-quality processing of subsequent optical signals.

II. Design and Analysis

The schematic diagram of the proposed dual-mode antenna transceiver integrated OPA structure is shown in Fig. 1. The structure can realize the functions of receiving and transmitting optical signals at the same time. It is divided into three modules, a 1×8 transmitter module, a 1×8 receiver module, and a 1×16 transmitter/receiver module. The overall structure can achieve twice the field view of the antenna through the dual-port opposite incidence. Under the 1×8 transmitter module, the optical signal is input into the optical waveguide through the grating coupler and evenly distributed by the MMI beam splitter array. Then the optical phase is modulated by the modulator array composed of Titanium heaters. Finally, the optical signal is emitted into free space through the corrugated grating antenna. Since the grating antenna is a wavelength-sensitive device, it can achieve two-dimensional control of the beam through lateral wavelength tuning and longitudinal phase tuning. Under the 1×8 receiver module, we adopted the coherent detection method. The reference light enters the waveguide through the grating coupler and is evenly distributed by the MMI beam splitting array. After modulation by the phase modulator, it is mixed with the received light signal through the directional coupler and enters the optoelectronics finally. The detector performs signal processing and can actively select the optical signal in the specified direction for processing by changing the phase of the reference light. In the 1×16 transmitter/receiver module, using the principle of reciprocity of light, the independent switching of receiving/transmitting mode is realized through 2×2 optical switches. Since the switch state is difficult to judge, it is necessary to connect a power monitor at the end of the optical switch to monitor the switch state in real-time.

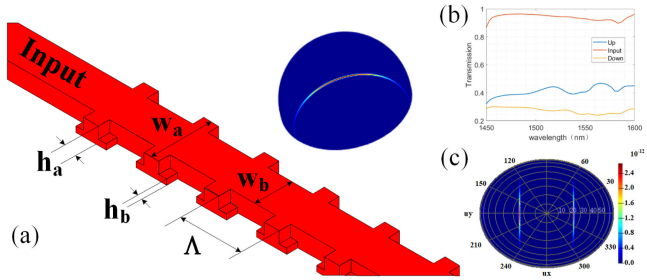

Fig. 2. (a) Corrugated Antenna Structure. (b) The transmission efficiency of the antenna. (c) Antenna far-field with single side incidence.

There are two main ways to design waveguide grating antennas, top-etched antennas, and edge-etched antennas. Considering that the edge etching antenna structure can reduce the contact area between the mode field and periodic defects and further reduce the crosstalk between adjacent antennas, we can obtain a more compact antenna array arrangement by adopting this structure. It can realize a higher collection efficiency in the receiving mode while increasing the scanning range of the antenna. Therefore, we finally chose to optimize the design of the edge-etched corrugated antenna structure. In addition, considering the reciprocity of the antenna [14], the higher the far-field emission efficiency is, the higher the receiving efficiency is under the same conditions. Therefore, we added the T-shaped etching structure of the antenna teeth, which further increases the energy diffracted by the antenna into the free space. At the same time, this structure can reduce the crosstalk between the antennas, and obtain a larger scanning range. The designed antenna structure is shown in Fig. 2(a). We choose the design with $\Lambda = 0.8\ \mu$m, the duty ratio is 0.5, $W_a = 0.5\ \mu$m, $W_b = 0.8\ \mu$m, $h_a = 0.22\ \mu$m, $h_b = 0.07\ \mu$m. Finally, the upward diffraction efficiency of the antenna in the wavelength range of 1470–1580 nm is more than 40%, and the upward diffraction efficiency at the peak wavelength is close to 50%. Fig. 2(b)–(c) shows the antenna diffraction efficiency diagram and far-field diagram at 1550 nm wavelength.

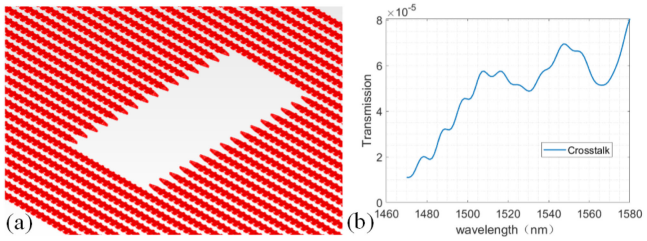

Fig. 3. (a) Optical partitions and terminations. (b) Crosstalk to the other side antenna.

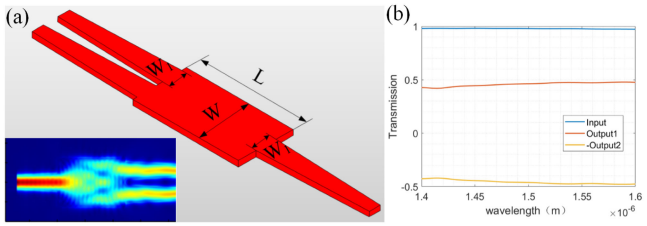

Fig. 4. (a) Schematic diagram of MMI structure. (b) Transmission efficiency of MMI.

In addition, for the 1x16 transmit/receive modules, since the optical receiving/transmitting signals need to be processed at the same time, the transmitting signal on the incident side will interfere with the receiving optical signal on the other side. Therefore, it is necessary to set a partition in the middle of the antenna and an optical terminal to achieve energy depletion, as shown in Fig. 3(a). We have simulated the crosstalk caused by the transmitting antenna to the receiving antenna. The results show that the antenna achieves less than 2% light energy transmission in the middle of the antenna, and the crosstalk caused by this design is more than 41 dB for the opposite antenna, as shown in Fig. 3(b). Since the power that the waveguide can withstand is limited, the energy transmitted from the transmitting antenna to the detector is weak. It is difficult to have a high enough sensitivity to respond to this signal, so the impact on other antennas is negligible.

Since we use wavelength tuning to achieve beam deflection in the longitudinal direction, it requires a larger bandwidth of the involved device. Therefore, we use a multi-mode interference (MMI) beam splitter array to achieve the 1 × 32 beam uniform distribution. MMI adopts the principle of multi-mode interference self-image imaging. The single or multiple images of input light will be formed repeatedly at periodic intervals along the propagation direction. We use symmetrical restricted interference to achieve uniform distribution of the beam 1 × 2. The imaging position obeys the following formula [15]:

$$L = \frac{3L_\pi}{4N} \tag{1}$$

Where L_π is the beat length of the two lowest-order modes, and N is the number of imaging. The formula can estimate the theoretical position of imaging roughly. On this basis, we simulated and optimized the actual imaging position and added a taper structure at the port position to minimize the insertion loss of the device. Fig. 4(a) shows the specific structure and optical

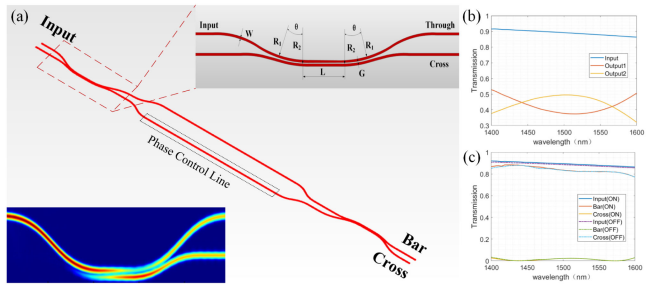

Fig. 5. (a) Schematic diagram of curved waveguide directional coupler and 2 × 2 optical switch based on the directional coupler. (b) Transmission efficiency of curved waveguide directional couplers. (c) Transmission efficiency of the 2 × 2 Optical Switch.

field energy distribution. We choose the design with W = 2.5 μm, L = 5.9 μm, W_1 = 0.8 μm. It can achieve the single-pass 47.55%, 47.65% transmittance at 1580 nm and 45.39%, 45.48% at 1470nm, as shown in Fig. 4(b). The unevenness is less than 0.01 dB, and the insertion loss of the beam splitter in the wavelength range of 1470–1580 nm is kept <0.32 dB after simulation optimization.

At the same time, we designed a thermo-optical switch based on the directional coupler. As shown in Fig. 5, since the conventional directional coupler has a strong wavelength dependence, we improve the wavelength dependence of directional couplers by introducing the curved waveguides [16]. Its working principle can be analyzed according to the coupled-mode theory and the asymmetric directional coupler theory. When the optical signal is input from the input port of the directional coupler, the output power of the through and cross output ports is:

$$P_{\text{cross}} = \frac{\kappa_c^2}{\delta^2}\sin^2(\delta \cdot L_c) \tag{2}$$

$$P_{through} = 1 - P_{cross} \tag{3}$$

Where L_c is the length of the coupling region, determined by the coupling angle θ and the bending radius R, κ_c is the coupling coefficient, and the value of δ is given by the following formula:

$$\delta = \sqrt{\left(\frac{\beta_1 - \beta_2}{2}\right)^2 + \kappa_c^2} \tag{4}$$

Where β_1 and β_2 are the propagation constants of the straight-through waveguide and the crossed waveguide respectively. For the traditional straight waveguide directional coupler, $\beta_1 = \beta_2$, the transmission spectrum changes linearly. When introducing a curved waveguide, $\beta_1 \neq \beta_2$, the transmission spectrum changes in a parabolic shape, so it can make the power coefficient of the directional coupler maintained around 50% over a wide wavelength range by optimization. Therefore, we introduce a curved waveguide structure according to this principle to widen the bandwidth. Fig. 5(a) shows the specific structure. We choose the design with L = 6.1 μm, G = 100nm, W = 0.5 μm, R_1 = 29 μm, R_2 = 29.6 μm, $\theta = 12°$. Fig. 5(b) shows the transmittance of the coupler varies with wavelength, achieving an additional loss of <0.81 dB and an extinction ratio of >7.44 dB in the

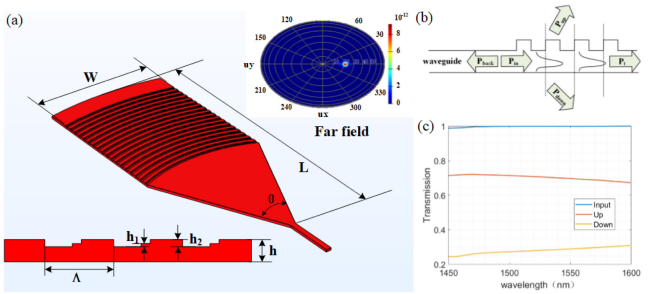

Fig. 6. (a) The grating coupler structure and its far-field distribution. (b) Schematic diagram of grating diffraction principle. (c) Transmission efficiency of the grating couplers.

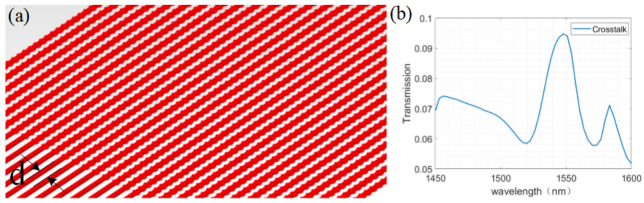

Fig. 7. (a) The antenna array arrangement. (b) Crosstalk between adjacent antennas.

operating bandwidth range. In addition, we designed a 2 × 2 Mach-Zehnder optical switch based on the curved waveguide directional coupler, as shown in Fig. 5(a). The optical signal is output through the Bar port when the switch is in the on-state. At this time, the additional loss in the operating wavelength range is less than 0.8 dB. The optical signal is output from the Cross port when the switch is in the off state, and the transmission of the Bar port is more than 13 dB. Fig. 5(c) shows the transmission efficiency of each state.

The grating coupler followed the Bragg diffraction conditions as shown in Fig. 6(b). For the traditional Bragg grating, the diffraction energy of the incident optical signal to the free space and the substrate is equal due to the symmetry of the structure. Therefore, we optimized the traditional structure by using a multi-layer shallow etching scheme to break the symmetry of the grating structure. It can reduce the loss of the grating coupler entering the Si-substrate and improve the upward diffraction efficiency of the antenna. In addition, in the coupling process between grating and fiber, the more concentrated the far-field energy distribution of the grating coupler is, the higher the coupling efficiency is. The far-field energy of the traditional straight waveguide grating coupler is more dispersed. Therefore, we use the curved waveguide grating structure to make the far-field energy of the grating more concentrated, which provides a reliable guarantee for the high-efficiency coupling between the grating coupler and the fiber. Fig. 6(a) shows the specific parameters of the grating coupler. After optimization, we choose the design with $\Lambda = 0.675$ μm, h = 0.22 μm, $h_1 = 0.04$ μm, $h_2 = 0.07$ μm, $\theta = 50°$, L = 36 μm, W = 13 μm. The design also considers the bandwidth. As shown in Fig. 6(c), it can provide upward diffraction efficiency of more than 66% in the wavelength range of 1470nm to 1580nm, and the diffraction efficiency can reach 72% at the peak wavelength. The incident loss to the substrate is less than 25%. The high upward diffraction efficiency provides a reliable guarantee for the high coupling efficiency between the grating and the chip.

For the antenna array, we use a linear and uniform arrangement with a 1.5 μm spacing. Due to the T-shaped etching structure of the antenna teeth, the crosstalk between antennas is reduced, and the antenna's upward diffraction efficiency is improved. Therefore, a small antenna spacing can be used to achieve a large scanning range. As shown in Fig. 7(b), we can see that under the 1.5 μm spacing, the crosstalk between adjacent antennas is more than 20 dB. Therefore, we can use this spacing to make the antennas linearly arranged, as shown in Fig. 7(a). In the receiving mode, the simulation shows that a large amount of energy will inevitably enter the substrate during the receiving process. Therefore, under the premise of avoiding excessive antenna crosstalk, the denser the array arrangement, the larger the effective receiving area and the higher the receiving efficiency. We define the effective acquisition efficiency:

$$\eta = \frac{A_{eff}}{A_t} \tag{5}$$

Where A_{eff} is the effective collection area of the antenna, and A_t is the overall antenna array aperture. We can achieve an effective collection efficiency of 43.3% per unit area.

For the scanning of the antenna array in the longitudinal range, it is realized by controlling the wavelength tuning. The longitudinal deflection angle is given by the following formula:

$$\sin\theta = \frac{n_{eff}\Lambda - \lambda_0}{\Lambda} \tag{6}$$

Where Λ is the period of the grating, λ_0 is the free space wavelength, and n_{eff} is the effective index of the guided mode. Therefore, we can achieve any angle of deflection in the far-field by adjusting the wavelength range or modifying the antenna period.

For the scanning of the antenna array in the lateral range, it is realized by applying equally spaced phase differences through the phase modulation array. Its scanning range can be given by the following formula:

$$\theta_s = 2\arcsin\left(\frac{\lambda}{2d}\right) \tag{7}$$

Where λ is the input wavelength and d is the antenna spacing.

The simulations show that we can achieve a scanning range of 15.6°+15.6° in longitudinal wavelength tuning and a scanning range of 62.2° in lateral phase tuning in the transmitting mode. Fig. 8 shows the far-field scanning diagrams of each direction of the OPA.

The result of the simulation shows that we can achieve an overall optical loss of less than 9.1 dB (including the waveguide loss of 2 dB/cm) in the transmitting mode without considering the grating coupling loss and the actual processing error loss. In the simulation process, we use the radius of 90° waveguide

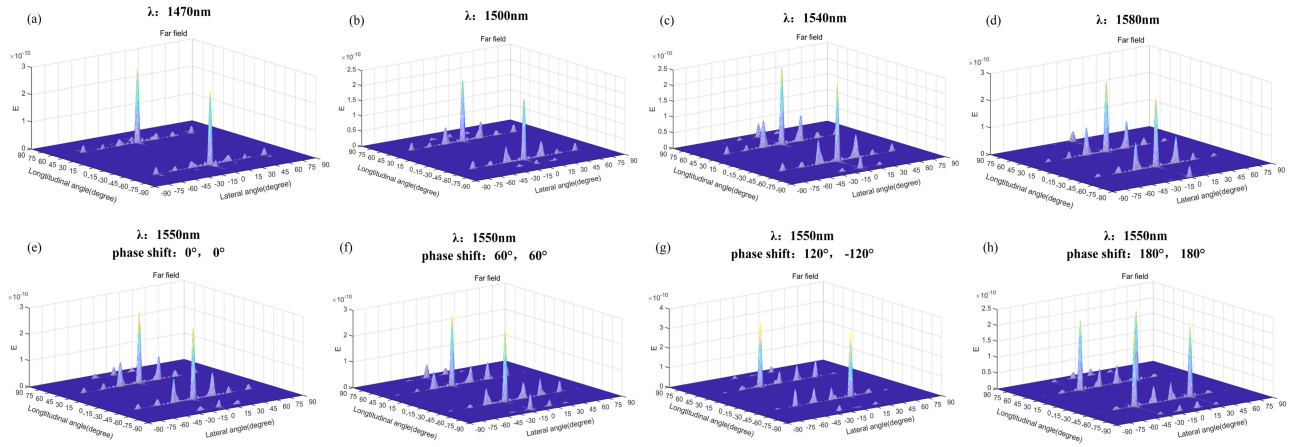

Fig. 8. (a)–(d) Antenna array far-field distribution at different wavelengths. (e)–(h) Antenna array far-field distribution under different phase differences.

bending more than 10 μm. The simulation shows that the bending loss of the waveguide is less than 0.04 dB. In addition, we can achieve a collection efficiency of 43.3% per unit area in the receiving mode, which provides a reliable guarantee for subsequent high-quality signal processing.

III. Conclusion

In conclusion, we have proposed an integrated design of the OPA transceiver based on the dual-mode corrugated antenna, which can realize the precise scanning of the OPA in two dimensions of 31.2° × 62.2° through longitudinal wavelength tuning and lateral phase tuning. The combination of the two detection methods can improve the detection accuracy while ensuring the system's receiving sensitivity. We can switch the OPA receiving and transmitting modes arbitrarily by designing the optical switch. At the same time, we have optimized the design of each optical device of the OPA. According to the statistics, the overall optical loss is less than 9.1 dB in the transmitting mode. The effective receiving area per unit area is more than 43.3% in the receiving mode, which provides a reliable guarantee for the high-quality processing of subsequent optical signals. What's more, the transceiver integrated structure can realize the simultaneous processing of the receive optical signal and the transmit optical signal, while can greatly improve the optical communication efficiency.

References

[1] S. Zhao, J. Chen, and Y. Shi, "Dual polarization and bi-directional silicon-photonic optical phased array with large scanning range," *IEEE Photon. J.*, vol. 14, no. 2, Apr. 2022, Art. no. 6620905.

[2] S. Emara et al., "Single-pixel imaging using carrier-depletion optical phased array with reduced phase shift requirement," *IEEE Photon. J.*, vol. 13, no. 5, Oct. 2021, Art. no. 6600105.

[3] C. V. Poulton et al., "Coherent solid-state LIDAR with silicon photonic optical phased arrays," *Opt. Lett.*, vol. 42, no. 20, pp. 4091–4094, Jun. 2017.

[4] H. -W. Rhee et al., "32 Gbps data transmission with 2D beam-steering using a silicon optical phased array," *IEEE Photon. Technol. Lett.*, vol. 32, no. 13, pp. 803–806, Jul. 2020.

[5] J. Zhou, S. Jie, A. Yaacobi, C. V. Poultonet, and M. R. Watts, "Design of 3D hologram emitting optical phased arrays," in *Proc. Adv. Photon.* 2015, Paper IT4A.7.

[6] X. Yan, J. Chen, D. Dai, and Y. Shi, "Polarization multiplexing silicon-photonic optical phased array for 2D wide-angle optical beam steering," *IEEE Photon. J.*, vol. 13, no. 2, Apr. 2021, Art. no. 6600506.

[7] D. Kwong et al., "On-chip silicon optical phased array for two-dimensional beam steering," *Opt. Lett.*, vol. 39, no. 4, pp. 941–944, Feb. 2014.

[8] J. K. Doylend, M. J. R. Heck, J. T. Bovington, J. D. Peters, L. A. Coldren, and J. E. Bowers, "Two-dimensional free-space beam steering with an optical phased array on silicon-on-insulator," *Opt. Exp.*, vol. 19, no. 22, pp. 21595–21604, Oct. 2011.

[9] J. Sun et al., "Large-scale silicon photonic circuits for optical phased arrays," *IEEE J. Sel. Topics Quantum Electron.*, vol. 20, no. 4, Jul./Aug. 2014, Art. no. 8201115.

[10] F. Zhang, D. Zhang, and S. Pan, "Fast and wide-range optical beam steering with ultralow side lobes by applying an optimized multi-circular optical phased array," *Appl. Opt.*, vol. 57, no. 18, pp. 4977–4984, 2018.

[11] J. Sun et al., "Two-dimensional apodized silicon photonic phased arrays," *Opt. Lett.*, vol. 39, no. 2, pp. 367–370, 2014.

[12] H. Abediasl and H. Hashemi, "Monolithic optical phased-array transceiver in a standard SOI CMOS process," *Opt. Exp.*, vol. 23, no. 5, pp. 6509–6519, 2015.

[13] R. Fatemi, B. Abiri, A. Khachaturian, and A. Hajimiri, "High sensitivity active flat optics optical phased array receiver with a two-dimensional aperture," *Opt. Exp.*, vol. 26, no. 23, pp. 29983–29999, 2018.

[14] R. Fatemi, P. P. Khial, A. Khachaturian, and A. Hajimiri, "Breaking FOV-aperture trade-off with multi-mode nano-photonic antennas," *IEEE J. Sel. Topics Quantum Electron.*, vol. 27, no. 1, Jan./Feb. 2021, Art. no. 6100614, doi: 10.1109/JSTQE.2020.3026966.

[15] L. B. Soldano and E. C. M. Pennings, "Optical multi-mode interference devices based on self-imaging: Principles and applications," *J. Lightw. Technol.*, vol. 13, no. 4, pp. 615–627, Apr. 1995.

[16] S. Chen, Y. Shi, S. He, and D. Dai, "Low-loss and broadband 2 × 2 silicon thermo-optic Mach–Zehnder switch with bent directional couplers," *Opt. Lett.*, vol. 41, no. 4, pp. 836–839, 2016.